

Thermal and thermomechanical properties of poly[(butylene succinate)-*co*-adipate] nanocomposite

Suprakas Sinha Ray^{a,b,*}, Jayita Bandyopadhyay^b, Mosto Bousmina^{b,**}

^a *Macromolecular Nanotechnology Research Group, National Centre for Nanostructured Materials, CSIR Materials Science and Manufacturing, 1-Meiring Naude Road, Brummeria PO Box 395, Pretoria 0001, South Africa*

^b *Department of Chemical Engineering, Laval University (CREPEC), Quebec, Canada G1K 7P4*

Received 8 November 2006; received in revised form 30 January 2007; accepted 3 February 2007

Available online 14 February 2007

Abstract

In this article the thermal and thermomechanical properties of neat poly[(butylene succinate)-*co*-adipate] (PBSA) and its nanocomposite are reported. Nanocomposite of PBSA with organically modified synthetic fluorine mica (OSFM) has been prepared by melt-mixing in a batch mixer. The structure of nanocomposite is characterized by X-ray diffraction patterns and transmission electron microscopic (TEM) observations that reveal homogeneous dispersion of intercalated silicate layers in the PBSA matrix. The melting behavior of pure polymer and nanocomposite samples are analyzed by differential scanning calorimetry (DSC), which shows multiple melting behavior of the PBSA matrix. The multiple melting behavior of the PBSA matrix is also studied by temperature modulated DSC (TMDSC) and wide-angle XRD (WXR) measurements. All results show that the multiple melting behavior of PBSA is due to the partial melting, re-crystallization, and re-melting phenomena. The investigation of the thermomechanical behavior is performed by dynamic mechanical thermal analysis. Results demonstrate substantial enhancement in the mechanical properties of PBS, for example, at room temperature, storage flexural modulus increased from 0.5 GPa for pure PBS to 1.2 GPa for the nanocomposite, an increase of about 120% in the value of the elastic modulus. The thermal stability of nanocomposite compared to that of neat PBSA is also examined in pyrolytic and thermo-oxidative conditions. It is then studied using kinetic analysis. It is shown that the stability of PBSA is increased moderately in the presence of OSFM.

© 2007 Elsevier Ltd. All rights reserved.

Keywords: Poly[(butylene succinate)-*co*-adipate]; Organically modified synthetic fluorine mica; Nanocomposite; Thermal and thermomechanical properties

1. Introduction

Over the last two decades, polymer nanocomposites based on organically modified layered silicate (OMLS) have received significant research attention, because they often exhibit concurrent improvement of mechanical, thermal, optical, and physicochemical properties when compared with

the pure polymer or conventional composites (micro- and macro-composites) [1–5]. In general, it is believed that these concurrent property improvements in nanocomposites come from interfacial interactions between the polymer matrix and OMLS as opposed to the conventional composites. The layered silicates have a layer thickness in the order of ~1 nm and very high aspect ratio (10–1000). A few weight percent of layered silicate, which are well dispersed throughout the polymer matrix, thus create much more surface area for polymer/filler interaction than do conventional composites [1,2].

In recent years, synthetic aliphatic polyesters have received much research attention for the production of high-performance, environment-benign biodegradable plastics [6,7]. These are generally made by polycondensation methods and raw materials are obtained from petrochemical feed stocks.

* Corresponding author. Macromolecular Nanotechnology Research Group, National Centre for Nanostructured Materials, CSIR Materials Science and Manufacturing, 1-Meiring Naude Road, Brummeria PO Box 395, Pretoria 0001, South Africa. Tel.: +27 012 841 2388; fax: +27 012 841 2135.

** Corresponding author.

E-mail addresses: rsuprakas@csir.co.za (S.S. Ray), bousmina@gch.ulaval.ca (M. Bousmina).

Unlike other petrochemical-based resins that take centuries to degrade after disposal, these polymers break down rapidly into carbon dioxide, water, and humus in appropriate conditions when they are exposed to the combined attack of water and micro-organisms [8,9]. These products also meet advanced composting standards and typically break down in 12 weeks under aerobic conditions [10].

In this direction, poly[(butylenesuccinate)-*co*-adipate] (PBSA) is among the most promising polymer. PBSA is a random copolymer of poly(butylene succinate) (PBS) and shows a variety of interesting physical properties including biodegradability [11]. Fig. 1a represents the molecular structure of PBSA. It is synthesized by polycondensation of 1,4-butanediol in the presence of succinic and adipic acids with relatively low production cost and satisfactory mechanical properties similar to that of polyolefins [11]. PBSA, compared with poly(butylene succinate) (PBS), is more susceptible to biodegradation because of its lower crystallinity and more polymer chains' flexibility [12]. PBSA also has excellent processability, so that it can be processed in the field of textiles into melt blow, multifilament, monofilament, flat, and split yarn and also in the field of plastics into injection molded products, thus being a promising polymer for various applications [13]. Therefore, increasing our understanding of the various intrinsic properties of PBSA, coupled with the knowledge of how such properties can be improved to achieve suitability for the thermoplastics processing, manufacturing, and end-use requirements, has fuelled technological and commercial interest of PBSA.

Recently, we have reported on the characterization, mechanical, and rheological properties of various types of PBSA/organically modified montmorillonite (OMMT) nanocomposites [14,15]. In all cases the intrinsic properties of neat PBSA are concurrently improved after nanocomposite formation. In another recent publication, we have reported the effect of organically modified synthetic fluorine mica (OSFM) on the non-isothermal crystallization behavior, kinetics, and finally, cold crystallization behavior of PBSA [16]. The non-isothermal crystallization kinetics of the nanocomposite indicates that the incorporation of OSFM decelerates the

mechanism of nucleation and crystal growth of PBSA. This is attributed to the homogeneous dispersion of the silicate layers into the PBSA matrix. On the other hand, the homogeneous dispersion increases the cold crystallization temperature of the nanocomposite.

The main objective of this article is to report the unique melting behavior of neat PBSA and its nanocomposite with OSFM. Both conventional and temperature modulated differential scanning calorimetry have been used to study the melting behavior. The thermomechanical properties and thermal stability of neat PBSA and its nanocomposite are also studied.

2. Experimental section

2.1. Materials and sample preparation

PBSA used in this study was a commercial product from Showa High Polymer Ltd., Japan, with the designation BIONOLLE #3001. PBSA was dried under vacuum at 50 °C for 36 h prior to use. The organically modified synthetic fluorine mica (OSFM) used in this study was supplied by CO-OP Chemicals Ltd., Japan, and was synthesized by replacing Na⁺ in synthetic fluorine mica (SFM) (original thickness of ~1 nm and average length of 200–300 nm) of a cation exchange capacity (CEC) of 120 mequiv/100 g with *N*-(coco alkyl)-*N,N*-[bis(2-hydroxyethyl)]-*N*-methylammonium cation (see Fig. 1b) by ion exchange reaction.

Synthetic fluorine mica (trade name SOMASIF) used in this study was synthesized by heating a mixture of talc and Na₂SiF₆ for several hours in an electric furnace. Like montmorillonite (MMT), synthetic fluorine mica also belongs to the same general family of 2:1 layered or phyllosilicates. The only difference between MMT and SFM is that SFM [NaMg_{2.5}(Si₄O₁₀)F₂] contains 'F' groups on its surface [17]. The reason for choosing *N*-(coco alkyl)-*N,N*-[bis(2-hydroxyethyl)]-*N*-methylammonium modified synthetic fluorine mica as an OMLS in this study was due to the closest value of solubility parameter of the surfactant with that of PBSA. The solubility parameter (δ) for PBSA and organic modifier, *N*-(coco alkyl)-*N,N*-[bis(2-hydroxyethyl)]-*N*-methylammonium was roughly calculated from the group contribution methods of Fedors [18]. The values of δ for PBSA and surfactant are 23.8 and 22.5 J^{1/2} cm^{-3/2}, respectively.

The nanocomposite was prepared through melt-mixing using a twin rotor thermohaake-mixer (Polylab system) operated at 135 °C (set point) and a rotor speed of 60 rpm for 8 min. OSFM powder was slowly added after two and half minutes of melting of PBSA inside the mixer, which was considered as time zero. The amount of OSFM loading was fixed to 6 wt%. The obtained nanocomposite strands were then dried under vacuum at 65 °C for 7 h to remove any residual water. The dried nanocomposite sample was molded using a Carver laboratory press at 2 MPa at 135 °C for 3 min. The molded samples were cooled at room temperature and then annealed at 60 °C for 5 h to crystallize isothermally before being subjected to all experiments.

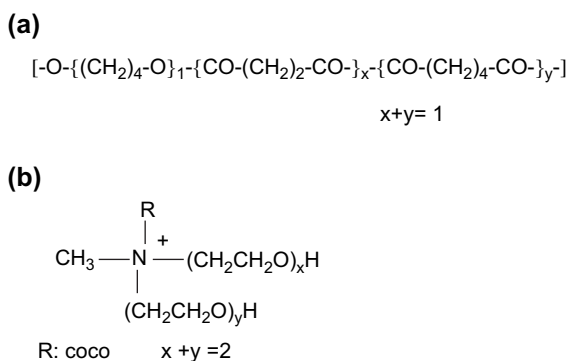


Fig. 1. (a) Molecular structure of poly[(butylene succinate)-*co*-adipate] (PBSA) and (b) chemical formula of the organic modifier used for the modification of synthetic fluorine mica (SFM).

2.2. Characterization techniques and property measurements

The molecular weight of PBSA before and after nanocomposite preparation with OSFM was determined by means of gel permeation chromatography (GPC, Viscotek, TDA 302), using polystyrene standards for calibration and chloroform as a carrier solvent at 35 °C with the flow rate of 1 mL/min. The thermal stability of both PBSA and surfactant used for the modification of pristine SFM were also verified by thermogravimetric analysis that did not reveal any degradation for 1 h at the mixing temperature.

XRD experiments were conducted on a Simens-500 diffractometer in the transmission mode. The beam was Cu K α radiation ($\lambda = 0.154$ nm) operated at 40 kV and 40 mA. The basal spacing ($d_{(001)}$) of OSFM before and after intercalation was estimated from the position of the (001) peak in the XRD pattern.

Dispersability of the intercalated silicate layers in the PBSA matrix was evaluated by means of TEM (JEOL model JEM-1230 instrument) operated at an accelerating voltage of 80 kV. The TEM specimens were about 70 nm thick. They were prepared by ultramicrotoming the nanocomposite sample encapsulated in epoxy matrix with a diamond knife.

Melting behaviors were studied on a TA Instruments DSC model Q100 series instrument under constant nitrogen flow. The DSC samples were weighed such that all the samples had identical PBSA content. The sample weight was maintained at low levels (3–4 mg) for all measurements in order to minimize any possible thermal lag during the scans. Each reported result is an average of four separate measurements. Temperature and heat of fusion were calibrated with an indium standard, and base line was checked according to TA Instruments protocols. The thermal history of both samples was the same.

To separate the heat capacity and kinetic related components during heating of neat PBSA and the nanocomposite, the TMDSC of the compression molded samples was carried out using the same DSC instrument with a constant nitrogen flow. TMDSC generally applies a sinusoidal temperature oscillation (modulation) on a conventional heating DSC and allows the total heat flow (as obtained from conventional DSC) to be separated into the heat capacity related (reversible) and kinetic (non-reversible) components. The heat capacity was calibrated with a sapphire sample. The heating rate was 2 °C, with an amplitude of ± 0.318 °C, and a period of 60 s.

Thermomechanical properties of neat PBSA and nanocomposite were measured by using a Rheometrics Scientific Analyzer (RSA) in the dual cantilever bending mode. The temperature dependence of storage flexural modulus (E'), loss modulus (E''), and $\tan \delta$ of neat PBSA and nanocomposite were measured at a constant frequency of 6.28 rad/s with the strain amplitude of 0.02% (selected after series of strain sweep tests at different temperatures) and in the temperature range of –65 to 75 °C at a heating rate of 2 °C/min.

The thermogravimetric analyses were conducted on a TGA Q500 instrument (TA Instruments) at a heating rate of 10 °C/

min under both pyrolytic and thermo-oxidation conditions, from room temperature to 700 °C. Sample (both PBSA and nanocomposite) weights were of (13 ± 0.6) mg and placed in open platinum pans. Typically, three consecutive runs were conducted for each sample and averages are reported with an uncertainty of ± 1.41 °C. For degradation kinetic analysis each sample was heated at five different heating rates of 5, 10, 15, 20, and 25 °C/min from room temperature to 700 °C under constant nitrogen flow (60 ml/min).

3. Results and discussion

3.1. Nanocomposite structure

Fig. 2 shows the result of XRD patterns of pure OSFM powder and corresponding PBSA/OSFM nanocomposite prepared with 6 wt% of OSFM. The characteristic mean inter-layer spacing of the (001) plane ($d_{(001)}$) for the OSFM powder is 2.06 nm ($2\theta = 4.29^\circ$). In the XRD pattern of the nanocomposite, the intensity of the characteristic peak of the OSFM is significantly reduced and a broad peak is observed at $2\theta = 2.82^\circ$ ($d_{(001)} = 3.13$ nm), indicating that the structure is potentially highly intercalated, due to the favorable interaction between the 'CO' group on the PBSA backbone with the hydroxyl groups present in the surfactant used for the modification of synthetic fluorine mica [16] (see Fig. 1a and b).

To support the XRD pattern, TEM observations are used to directly and qualitatively visualize the state of the silicate layers dispersion/delamination in the PBSA matrix. Fig. 3 shows the TEM bright field image of the nanocomposite corresponding to the XRD pattern as shown in Fig. 1, in which dark entities are the cross-section of intercalated OSFM layers. TEM image of the nanocomposite reveals that there are some intercalated stacked and disordered and/or exfoliated silicate

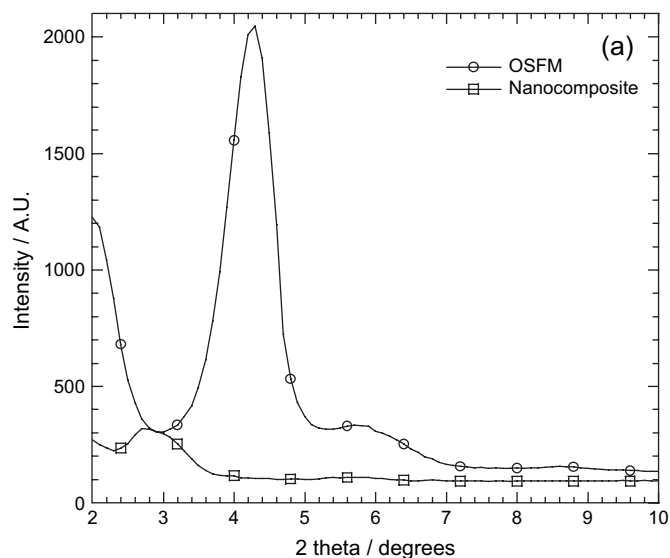


Fig. 2. X-ray diffraction (XRD) patterns of pure organically modified synthetic fluorine mica (OSFM) powder and an isothermally crystallized (50 °C for 5 h) compression molded nanocomposite sample (thickness was around 1 mm).

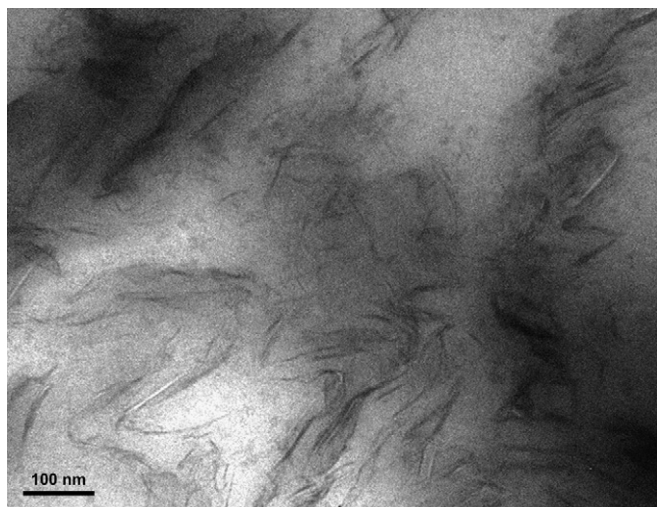


Fig. 3. Bright field transmission electron microscopy (TEM) images of the nanocomposite in which dark entities are the cross-section of intercalated OSFM layers.

layers coexisting in the nanocomposites. The stacked intercalated silicate layers are responsible for weak XRD diffractions as observed in Fig. 2 whereas the disordered and exfoliated silicate layers have no periodic stacking and thus remain XRD silent [19,20]. This kind of mixed intercalated and/or exfoliated structure originates from chemical and size inhomogeneities of the silicate layers. Typically the larger – in lateral size – silicate layers create a stacked intercalated structure, whereas the smaller layers tend to delaminate [19,20]. Details regarding structure can be found in Ref. [16].

3.2. Melting behavior

3.2.1. Compression molded samples

To understand the initial melting behavior and re-crystallization response of neat PBSA and nanocomposite samples, DSC analysis of compression molded samples were conducted at a heating rate of 10 °C/min and the relative first scans are shown in Fig. 4. Results are summarized in Table 1. To have identical thermal history of all samples, samples were kept at 50 °C for 3 h inside DSC, before starting each set of experiments. Samples were also weighed such that all the samples had identical PBSA content. The glass transition temperature (T_g) of neat PBSA ($T_g = -36$ °C) slightly increased after nanocomposite ($T_g = -34.4$ °C) formation with OSFM. This indicates moderate interaction between the PBSA matrix and OSFM surface. On the other hand, both samples show three endothermic melting peaks of PBSA, labelled as I, II, and III from the low to high temperature and one re-crystallization peak in between the last two melting peaks (see Fig. 4).

Multiple melting behaviors have already been reported in poly(ethylene terephthalate) [21], poly(butylene terephthalate) [22], polypropylene [23], semicrystalline polyimides [24], poly(ether ether keton) [25], poly(butylene succinate) [26–29] and various other polymers [30]. Recently, Wang et al. [31] reported the multiple melting behaviors of PBSA. However, they

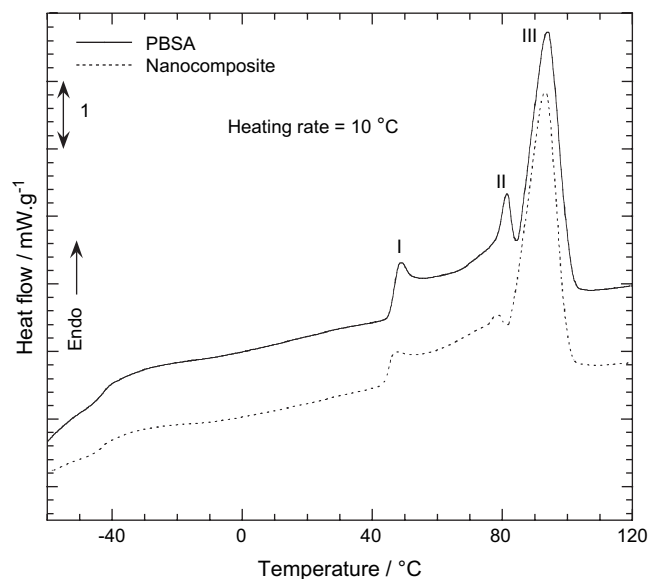


Fig. 4. First heating DSC thermograms of compression molded samples. Before starting each set of experiment sample was kept at 50 °C for 3 h inside the DSC. The samples were also weighed such that all the samples had identical PBSA content.

did not explain clearly why PBSA shows multiple melting endotherms. There are several models to explain the multiple melting behaviors of thermoplastic semicrystalline polymers, of which the two most important ones are: (a) the crystal structure modification during the heating scan and (b) the presence of melting, re-crystallization, and re-melting phenomena [32–34]. According to the second model, the first step is the melting and re-crystallization of the low melting crystallites with lower thermal stability and then the melting of the crystallites with higher thermal stability formed through the re-crystallization of the melting of the crystallites of the lower melting endotherms. Subsequent discussion in this section will consider the applicability of the above two reasons in addressing the multiple melting behaviors in light of the available experimental evidences.

To determine the formation of different crystal modification during heating scan which may be responsible for the multiple melting endotherms, wide-angle XRD (WXR) has been performed on neat PBSA sample crystallized (for 5 min) at above and below the temperature of each endotherm. The WXR scans in Fig. 5 show the results obtained for the compression molded sample (prior to the experiment, the sample was kept at 50 °C for 3 h) crystallized at 25, 70, 90, 110, 50, and 30 °C. It is clear from the figure that for the PBSA sample crystallized at six different temperatures no significant differences are visible in terms of position of the peak or the presence

Table 1
DSC data of neat PBSA and nanocomposite

Sample	$T_g/^\circ\text{C}$	$T_{ml}/^\circ\text{C}$	$T_{mII}/^\circ\text{C}$	$T_{mIII}/^\circ\text{C}$
PBSA	-36	49.0	81.5	94
Nanocomposite	-34.4	47.0	78.5	93

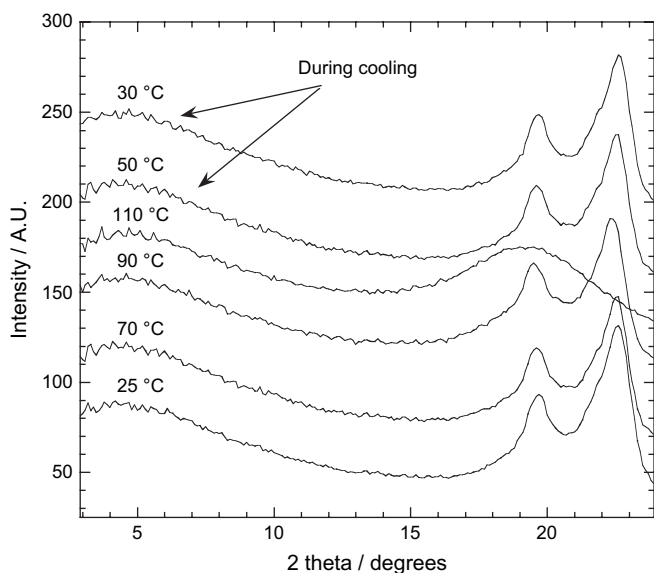


Fig. 5. Temperature dependence of WAXRD patterns of PBSA.

of new ones. However, the PET sample shows significantly different WAXRD patterns when crystallized at different temperatures [21a]. Therefore, on the basis of the WAXRD patterns, it is contended that the presence of the three prominent melting endotherms is not the result of the formation of different crystal structures during heating.

Now to verify the presence of melting, re-crystallization, and re-melting phenomena, both samples are scanned at different heating rates of 2, 5, 10, 15, and 20 °C/min. Results are presented in Fig. 6. In the case of PBSA with increasing the heating rate, the endotherm 'III' is shifted towards the lower temperature, but the endotherm 'I' becoming more prominent and systematically moves to the higher temperature region and another endotherm 'II' appearing in between two endotherms. Another interesting observation is that re-crystallization is becoming more important with heating rate. This indicates the melting–re-crystallization process being operative at the same time for higher endotherm. At a very slow heating rate, the sample passes through the re-crystallization process slowly, so there is more than enough time for the melted sample to reorganize into new crystals. For this reason, only endotherm 'III' perfectly appears at a very slow heating rate (2 °C/min). However, at higher heating rates (more than 2 °C/min); the sample passes through the re-crystallization region so rapidly that there is not enough time for the melted sample to reorganize into new crystals. For this reason, the reorganization process is largely inhibited as the heating rate increases and at the same time the amount of perfect crystals decreases, which finally contributes to the decrease in the peak temperature of endotherm 'III'. These observations indicate the presence of melting, re-crystallization, and re-melting phenomena which are responsible for the multiple melting behavior of PBSA.

The nanocomposite sample also shows the same type of melting behaviors. However, all the melting endotherms are shifted towards the lower temperature compared to the neat PBSA. Two possible effects may be evoked regarding the shift

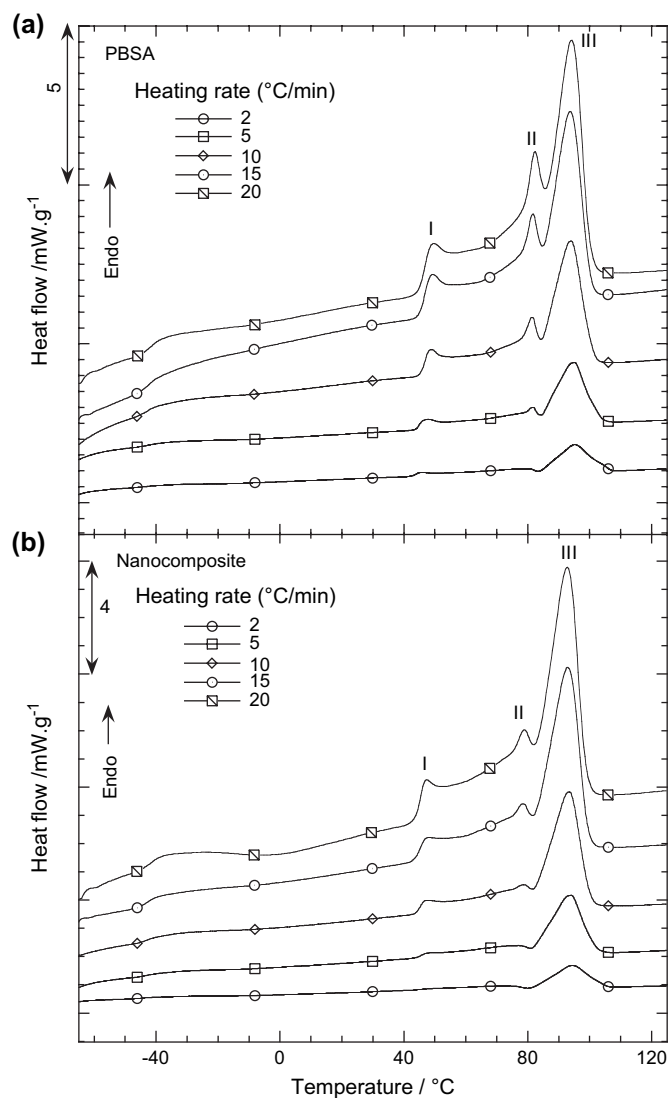


Fig. 6. Heating rate dependence of DSC thermograms of compression molded samples. Before starting each set of experiment sample was kept at 50 °C for 3 h inside the DSC. The samples were also weighed such that all the samples had identical PBSA content.

of melting endotherms towards the lower temperature region in the case of nanocomposite. The first one is the decrease in the matrix molecular weights after nanocomposite preparation with OSFM. To examine the fate of the PBSA matrix after nanocomposite preparation, GPC measurements of PBSA matrix before ($M_w = 119$ kg/mol; PDI = 1.026) and after nanocomposite preparation ($M_w = 114$ kg/mol; PDI = 1.029) were carried out. GPC data clearly indicate that there is almost no degradation of the PBSA matrix after nanocomposite preparation with OSFM. Therefore, matrix molecular weights are not responsible for the shift of melting endotherms towards the lower temperature in the case of nanocomposite. A second reason is the restricted polymer chain mobility. Because of the moderate interaction between the 'CO' groups present in PBSA backbone and hydroxyl groups in OSFM, polymer chains are highly intercalated into the silicate layers, which finally lead to the high level of homogeneous dispersion of

silicate layers into the PBSA matrix, as revealed by XRD patterns and TEM observations (see Figs. 2 and 3). This full dispersion of silicate layers acts as obstacle for the mobility and the flexibility of the polymer chains to fold and join the crystallization growth front. That means, the overall percent crystallization of the PBSA matrix decreases in the presence of OSFM [16]. For this reason, all endothermic peaks are less intense and shifted towards the lower temperature region than those of neat PBSA.

To further support the melting, re-crystallization, and re-melting phenomena of PBSA, TMDSC has been applied. TMDSC generally applies a sinusoidal temperature oscillation (modulation) on a heating conventional DSC and makes the total heat flow (as obtained from conventional DSC) to be separated into the heat capacity related (reversible) and kinetic (non-reversible) components. Therefore, TMDSC allows us to see that some re-crystallization process occurs as soon as PBSA begins to melt. Figs. 6 and 7 shows the TMDSC traces of neat PBSA and nanocomposite samples that are heated at a heating rate of 2 °C/min. For both samples total heat flow (middle curve) is separated into the well defined reversible heat flow (top curve) and the non-reversible heat flow (bottom curve) (Fig. 7). For neat PBSA sample, the following behaviors are observed: Firstly, the lower melting in the non-reversible signal curve begins at about 1 °C before the corresponding melting observed in the total curve. Secondly, the well-distinguished re-crystallization signal is recorded in both non-reversible and total heat flow curves, and at the same time the melting signal is observed in the reversible curve. Thirdly, the signal intensity of re-crystallization exotherm in the non-reversible signal is enhanced significantly compared to the exotherm recorded in the reversible and the total heat flow curves. This observation may be due to the continuous partial melting and perfection of crystals at temperatures before their final melting. Finally, double finger-like melting behavior appeared in the reversible heat flow curve. Generally, the gap between crystallization and final melting of the same crystals is usually larger than 2 °C, especially at large supercoolings like those observed in this case. Therefore, melting during the short heating step is rather expected to be reversible [35]. Another reason may be short chain segments, which remain attached to the crystal surfaces, set up local equilibria after all initial melting, re-crystallization, and reorganization is completed [36]. TMDSC curves of the nanocomposite also show the same types of behaviors as observed in the case of neat PBSA matrix but all endo- and exotherm signals are less intense and shifted towards the lower temperature region. This is again due to the restricted movement of the polymer chains in nanocomposite.

All the observations mentioned above in the case of both neat PBSA and nanocomposite samples confirm that the multiple melting behavior of PBSA originates from the melting and re-crystallization of the low melting crystallites with lower thermal stability. The high melting endotherm corresponds to the melting of the crystallites with higher thermal stability formed through the re-crystallization of the melting of the crystallites of the lower melting endotherms.

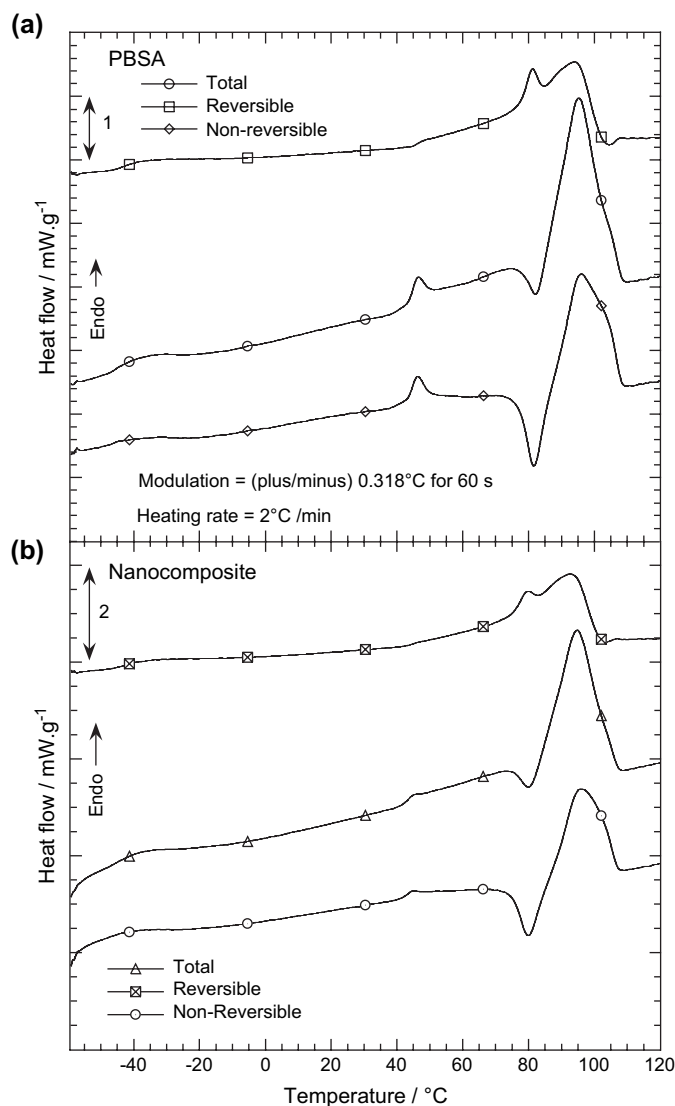


Fig. 7. First heating TMDSC of compression molded samples. Heating rate 2 °C/min, with an amplitude of ± 0.318 °C, and a period of 60 s. Before starting each set of experiment, the sample was kept at 50 °C for 3 h inside the DSC. The samples were also weighed such that all the samples had identical PBSA content.

3.2.2. Melting behavior after non-isothermal crystallization

To study the influence of cooling rate during non-isothermal crystallization on the melting behavior of PBSA, the samples have been heated at a rate of 20 °C/min directly from room temperature (25 °C) as soon as the cooling has finished. Parts 'a' and 'b' of Fig. 8, respectively, represent the subsequent melting behavior of PBSA and nanocomposite samples non-isothermally crystallized from the melt (150 °C) at the cooling rate ranging 1–20 °C/min. The total heat of fusion (ΔH_{en}) of two melting peaks of PBSA estimated by integration of the area under the endothermic region of the DSC thermograms, decreases with the addition of OSFM (see Table 2), indicating that the degree of crystallinity of PBSA is decreased by inorganic phase incorporation. Another interesting behavior is that for both samples, double melting endotherms and one small re-crystallization exotherm appear when crystallized

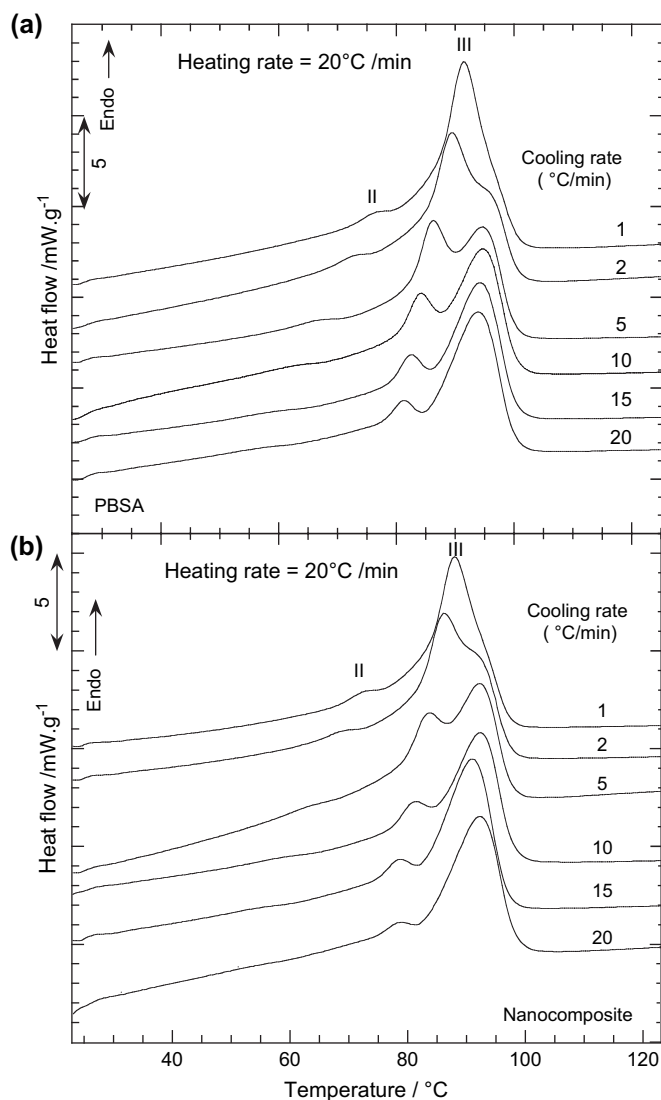


Fig. 8. Melting behavior of PBSA and nanocomposite samples after non-isothermal crystallization at different cooling rates.

Table 2

Cooling rate dependence of the total heat of fusion (ΔH_{en}) of two melting peaks of PBSA estimated by integration of the area under the endothermic region of the DSC thermograms

Sample	$\phi/^\circ\text{C min}^{-1}$	$\Delta H_{en}/\text{J g}^{-1}$ ^a
PBSA	1	92.0
	2	91.1
	5	79.5
	10	78.9
	15	77.1
	20	73.5
Nanocomposite	1	89.5
	2	88.3
	5	78.5
	10	77.3
	15	76.8
	20	72.7

^a ϕ is the cooling rate during non-isothermal crystallization from the melt.

^a Total heat of fusion of two melting peaks of PBSA evaluated from heating scans after non-isothermal crystallization. The DSC samples were weighed such that all the samples had identical PBSA content.

non-isothermally from the melt at a heating rate of 20 °C/min, while both samples show triple melting endotherms when compression molded samples are heated at the same heating rate. This result indicates that crystals associated with the 'I' melting endotherm do not form during non-isothermal crystallization at all cooling rates. On the other hand, endotherms 'II' and 'III' appear at the same temperature range for both samples (see Fig. 4).

In case of neat PBSA, endotherms 'II' and 'III' appear perfectly when the sample was crystallized non-isothermally at a cooling rate of 20 °C/min from the melt. However, with decreasing the cooling rate, the endotherm 'II' systematically shifts towards the higher temperature, whereas the endotherm 'III' moves in opposite direction. At a very slow cooling rate of 1 °C/min, the PBSA sample shows a perfect high temperature endotherm ('I') and a small shoulder of low temperature endotherm ('II'). On the other hand, the magnitude of the area of the endotherm 'II' increases and that of high melting endotherm ('III') decreases by decreasing the cooling rate. These observations indicate that with decreasing the cooling rate, the crystal growth associated with the low melting endotherm becomes more important and controls the melting behavior. This also supports reasons that the melting, recrystallization, and re-melting phenomena are responsible for the multiple melting behaviors of PBSA. The same behaviors are also observed in case of the nanocomposite sample, but all endotherms shift towards the lower temperature region. This is again due to the restricted movements of the polymer chains in nanocomposite.

3.3. Dynamic mechanical analysis

The dynamic mechanical analysis generally reveals the amount of energy stored in the nanocomposite as elastic energy and the amount of energy dissipated during mechanical strain, which strongly depends on the geometrical characteristics, and the level of dispersion of filler in the matrix. It also depends on the degree of interaction between the matrix and filler surface [37]. The temperature dependence of E' , E'' , and $\tan \delta$ of PBSA and nanocomposite are presented in Fig. 9. For the nanocomposite, a significant increase in E' with respect to that of the PBSA is observed over all the temperature ranges investigated. Table 3 summarized the E' values of neat PBSA and those of the nanocomposite at different temperature ranges. At low temperature both the PBSA matrix and the nanocomposite are in glassy state. The matrix T_g is not affected significantly by OSFM incorporation. However, over the entire measured temperature range, E' of the nanocomposite is always higher than that of the neat PBSA. This behavior may be due to the high degree of intercalation of polymer chains into the silicate layers of the OSFM (as observed in XRD patterns and TEM images, see Figs. 2 and 3), which leads to the large surface area for the favorable interactions between silicate layers and the polymer matrix. Polymer chains inside the silicate galleries are immobilized and the effect of immobilization on the polymers chains may be the main responsible factor for this substantial

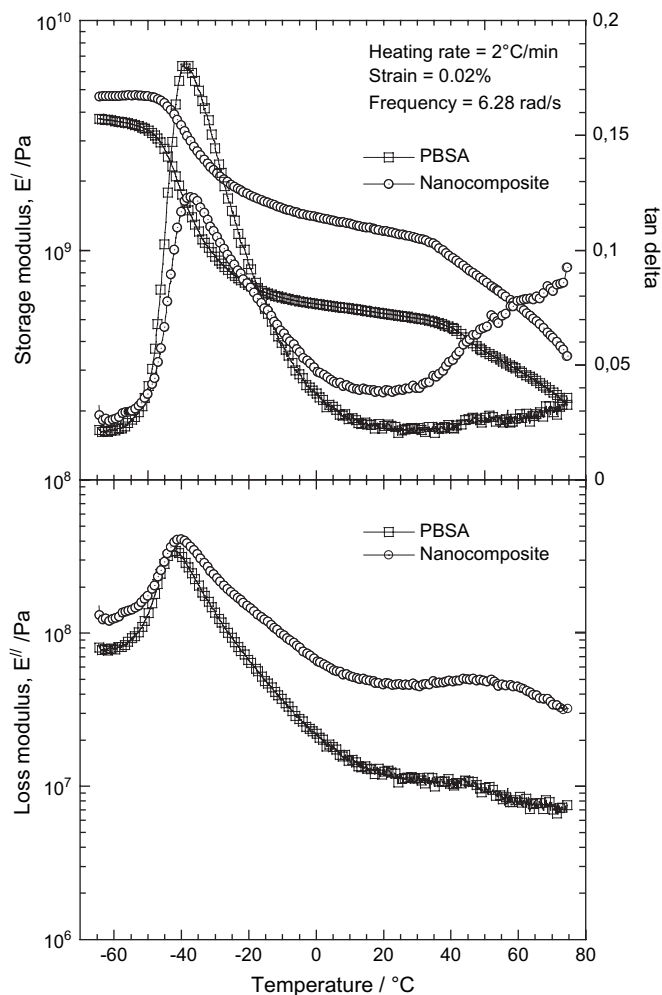


Fig. 9. Temperature dependence of storage flexural modulus (E'), loss modulus (E'') and loss $\tan \delta$ of PBSA and nanocomposite. Both samples were annealed at 50 °C for 3 h.

increase in E' . At room temperature (25 °C), the extent of increase in E' of nanocomposite is 140% compared to that of neat PBSA (Fig. 9a). The incorporation of OSFM in the PBSA matrix also results in a substantial increase in E'' as can be seen (Fig. 9b). This may be due to the presence of strong internal friction between homogeneously dispersed intercalated silicate particles. On the other hand, the temperature of loss $\tan \delta$ of PBSA, is generally considered as the matrix T_g , which is increased slightly (1.6 °C) after nanocomposite formation (see Fig. 9a). This again supports that there

Table 3
Temperature dependence of storage flexural modulus (E') of PBSA and nanocomposite

Sample	E' /GPa			
	−60 °C	−20 °C	25 °C	60 °C
PBSA	3.6	0.7	0.5	0.3
Nanocomposite	4.7 [30.5]	1.7 [142]	1.2 [140]	0.6 [100]

Value in the parentheses indicates the percent of improvement.

are some favorable interactions between the PBSA matrix and filler surfaces.

3.4. Thermogravimetric analysis

In this section the thermal stability of neat PBSA and nanocomposite in different atmospheres is discussed. In order to get information on the mode of action of OSFM on the degradation of the PBSA matrix, a non-reversible (kinetic) approach has been used. The detailed mechanisms of the degradation reactions of neat polymer or polymer in nanocomposite are generally unknown and in such cases, kinetic analysis of the reaction in the physical–chemical sense is not possible. When TGA is used for a kinetic study of a polymer degradation process, in fact, the rate of evaporation of degradation products is measured, but not the intrinsic chemical reaction rate such as breaking of bonds, etc. Again not every broken bond in the polymer chain leads to the evaporation of product, but only polymer chain fragments small enough to evaporate at the given reaction temperature will actually leave the polymer sample. This means that both physical and chemical processes influence the measured rate of change of the polymer mass and hence the observed degradation kinetics [38].

3.4.1. Thermal stability in different atmospheres

The TGA traces of the neat PBSA and nanocomposite in pyrolytic and thermo-oxidative conditions are presented in parts 'a' and 'b', respectively, of Fig. 10. The results are summarized in Table 4. The first derivative TGA (dTGA) curves are also shown in Fig. 10. The dTGA curves are chosen for the presentation because they more clearly show the difference in thermal stability between samples. It is clear from the figure that whatever the experimental conditions, the nanocomposite sample always shows higher overall thermal degradation temperature than that of the neat PBSA. The higher thermal stability of the nanocomposite can be attributed to the homogeneous dispersion of intercalated silicate layers which by nature has much higher thermal stability [39]. Under thermo-oxidative conditions (Fig. 10b), a small weight loss (~2.4 wt% in the temperature range of 225–335 °C) is observed, which can be assigned to the degradation of surfactant used for the modification of SFM [40]. However, the nanocomposite does not show such degradation in pyrolytic conditions. This suggests that the surfactant is more prone to degrade in thermo-oxidative conditions than pyrolytic conditions (Fig. 10a). Again under thermo-oxidative conditions, the onset degradation temperature (5 wt% loss) of the nanocomposite did not enhance significantly (5 °C). Under pyrolytic conditions, the onset degradation temperature increased moderately (~14 °C) more than that of neat PBSA. However, the main degradation temperature and char formation for the nanocomposite are increased in air compared to nitrogen. It is possible that the different types of char formation mechanism under oxidative environment, actually slow down the oxygen diffusion, thus hindering the oxidation procedure under thermo-oxidative conditions. This observation indicates improved flame retardance property of the nanocomposite.

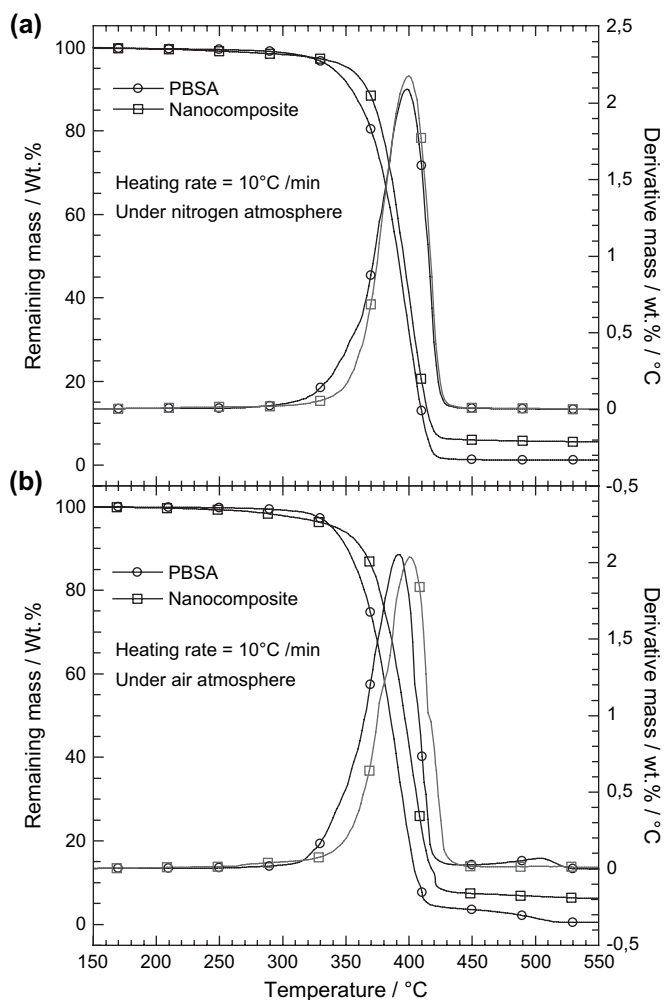


Fig. 10. TG and DTA curves of PBSA and nanocomposite in nitrogen and air atmospheres.

3.4.2. Kinetic analysis

For kinetic analysis of degradation of the polymer we have taken two assumptions: first one is that all reactions are irreversible. This is a very reasonable assumption because during degradation of polymeric material, the evolved gases are continuously removed by the gas flow from the TGA furnace. Another assumption is that the isothermal rate of conversion ($d\alpha/dt$) is a linear function of a temperature-dependent rate constant (k) and a temperature-independent function of the conversion (α), that is:

$$d\alpha/dt = kf(\alpha) \quad (1)$$

where $f(\alpha)$ depends on the particular degradation mechanism [41].

Therefore, according to Arrhenius,

$$k = Ae^{-E/RT} \quad (2)$$

where A is the pre-exponential factor and independent of temperature, E is the activation energy, R is the universal gas constant, and T is absolute temperature. Now if the sample temperature changed continuously at a controlled and constant heating rate,

$$\beta = dT/dt \quad (3)$$

the variation in the conversion can be analyzed as a function of temperature and this temperature being independent of the time of heating.

One of the most common methods to calculate activation energy during thermal degradation is the Kissinger method [42]. According to this method, E can be evaluated without knowing the precise reaction mechanism by the following equation:

$$\frac{d(\ln \beta/T_p^2)}{d(1/T_p)} = -\frac{E}{R} \quad (4)$$

where T_p is the temperature corresponding to the inflection point of the thermal degradation curves, i.e. maximum reaction rate. From a plot of $\ln(\beta/T_p^2)$ versus $1/T_p$, and fitting to a straight line, E can be easily calculated from the slope.

To determine T_p values, each sample has been heated at five different heating rates of 5, 10, 15, 20, and 25 °C/min from room temperature to 700 °C under constant pure nitrogen flow (60 ml/min). Heating rate dependence of the first derivative TGA (dTGA) curves of neat PBSA and nanocomposite are shown in Fig. 11. The values of T_p are tabulated in Table 5. E can be calculated from the slope of a plot of $\ln(\beta/T_p^2)$ versus $1/T_p$ (see Fig. 12) and data are presented in Table 5. It is clear from the data presented in Table 5 that the activation energy of the thermal degradation for the nanocomposite is slightly higher than that of neat PBSA. This increasing tendency of activation energy of the nanocomposite is consistent with the results described in the previous section.

4. Conclusions

In the present study we have systematically investigated the effect of OSFM on the melting behavior, thermomechanical properties and finally, the thermal stability of biodegradable

Table 4
TGA results of thermal degradation of PBSA and nanocomposite

Sample	Under nitrogen				Under air			
	$T_{5\%}/^{\circ}\text{C}$	$T_{50\%}/^{\circ}\text{C}$	$T_{85\%}/^{\circ}\text{C}$	Residue at 550 °C	$T_{5\%}/^{\circ}\text{C}$	$T_{50\%}/^{\circ}\text{C}$	$T_{85\%}/^{\circ}\text{C}$	Residue at 550 °C
PBSA	338.3	392.1	408.5	1.0	339.5	386.2	402.6	0.3
Nanocomposite	352.3	396.8	413.2	5.6	344.1	396.8	416.7	6.0

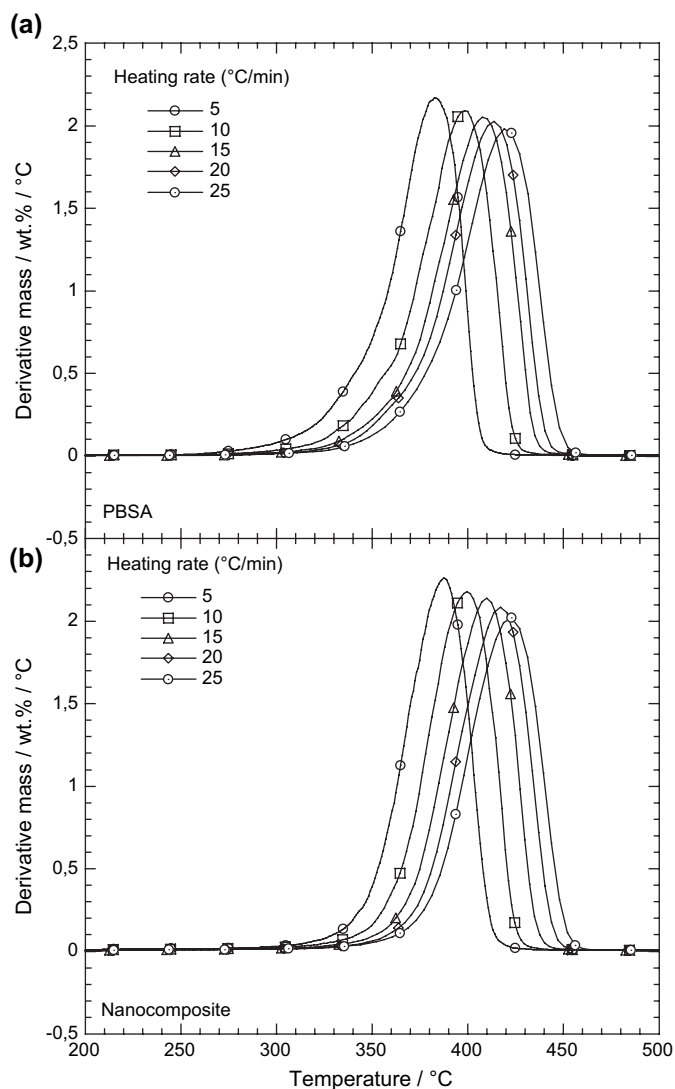


Fig. 11. Heating rate dependence of DTA curves of PBSA and nanocomposite under pure nitrogen flow.

PBSA. The PBSA nanocomposite based on OSFM has been prepared by melt-mixing in batch mixer. XRD patterns and TEM observations reveal a homogeneous dispersion of intercalated silicate layers in the PBSA matrix. Both conventional and temperature modulated differential scanning calorimetry

Table 5
Activation energy (E) of neat PBSA and nanocomposite samples calculated by using Kissinger method

Heating rate, $\beta/^\circ\text{C min}^{-1}$	Sample		Sample	
	PBSA		Nanocomposite	
	$T_p/^\circ\text{C}$	$\ln(\beta/T_p^2)$	$T_p/^\circ\text{C}$	$\ln(\beta/T_p^2)$
5	383.4	-11.36	388.3	-11.38
10	399.2	-10.72	400.9	-10.73
15	408.3	-10.34	410.8	-10.36
20	414.2	-10.07	417.5	-10.08
25	420.1	-9.86	423.3	-9.9
$E/\text{kJ mol}^{-1}$	159.9		168.9	

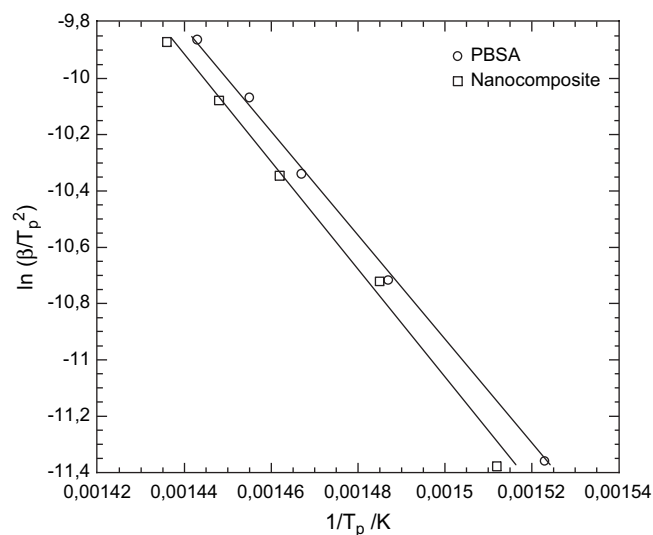


Fig. 12. Determination of the activation energy, E describing the thermal degradation process of PBSA and nanocomposite based on Kissinger method.

have been used to study the melting behavior of PBSA and its nanocomposite. For both samples multiple melting behavior is observed and it is associated with partial melting, recrystallization, and re-melting phenomena. Neat PBSA sample always exhibits higher melting temperature and heat of fusion. On the other hand, the nanocomposite is characterized by a lower melting temperature and heat of fusion. These are due to the homogeneous dispersion of OSFM particles in the PBSA matrix. The homogeneous dispersion of OSFM particles in the PBSA matrix might hinder the local lamellar crystallization and leads to the decrease in overall degree of crystallinity and hence lower melting temperature.

The full dispersion of OSFM particles in PBSA matrix leads to the dramatic improvement in elastic storage modulus but very moderate improvement in loss modulus of neat PBSA. The thermal stability of the nanocomposite is also studied and described using a kinetic analysis. The stability of PBSA is moderately increased in the presence of OSFM under both nitrogen and air atmospheres.

Acknowledgement

The authors thank Mr. K. Okamoto of the NMRI, Nagoya, Japan for PBSA sample. We express our appreciation to the reviewers for their constructive and meticulous assessment of the manuscript. MB thanks the Natural Sciences and Engineering Research Council of Canada (NSERC) for financial support.

References

- [1] Sinha Ray S, Bousmina M. Prog Mater Sci 2005;50:962.
- [2] Sinha Ray S, Okamoto M. Prog Polym Sci 2003;28:1539.
- [3] Biswas M, Sinha Ray S. Adv Polym Sci 2001;55:167.
- [4] Alexander M, Dubois Ph. Mater Sci Eng 2000;R28:1.
- [5] Giannelis EP. Adv Mater 1996;8:29.

- [6] Edlund U, Albertsson AC. Degradable aliphatic polyesters, vol. 157. Berlin: Springer; 2002.
- [7] Zhao J-H, Wang XQ, Zeng J, Yang G, Shi FH, Yan Q. Polym Degrad Stab 2005;90:173.
- [8] Uchida H, Nakajima-Kambe T, Shigeno-Akutsu Y, Nomura N, Tokiwa Y, Nakahara T. FEMS Microbiol Lett 2000;189:25.
- [9] Teeraphatpotnchai T, Nakajima-Kambe T, Shigeno-Akutsu Y, Nakayama M, Nomura N, Tokiwa Y, et al. Biotechnol Lett 2003;25:23.
- [10] Hayase N, Yano H, Kudoh E, Tsutsumi C, Ushio K, Miyahara Y. J Biosci Bioeng 2004;97:131.
- [11] Ishioka DR, Kitakuni E, Ichikawa Y. In: Doi Y, Steinbuechel A, editors. Aliphatic polyesters: 'Bionolle'. Biopolymers, Polyesters III. Application and commercial products, vol. 4. Weinheim: Wiley-VCH Verlag GmbH; 2002. p. 275.
- [12] Nikolich MS, Djonlagic J. Polym Degrad Stab 2001;74:263.
- [13] Fujimaki T. Polym Degrad Stab 1998;59:209.
- [14] Sinha Ray S, Bousmina M. Polymer 2005;46:12430.
- [15] Sinha Ray S, Bousmina M, Okamoto K. Macromol Mater Eng 2005;290:759.
- [16] Sinha Ray S, Bousmina M. Macromol Chem Phys 2006;207:1207.
- [17] Data sheet, CO-OP Chemical Ltd., Japan.
- [18] Krevelen DWV. Properties of polymer. Amsterdam, The Netherlands: Elsevier; 1990.
- [19] Dritis VA. X-ray diffraction by disordered lamellar structures. New York: Springer; 1990. p. 21.
- [20] Sinha Ray S, Yamada K, Okamoto M, Ogami A, Ueda K. Chem Mater 2003;15:1456.
- [21] (a) Qiu G, Tang Z, Huang N, Gerking L. J Appl Polym Sci 1998;69:729; (b) Tan S, Su A, Li W, Zhou E. Macromol Rapid Commun 1998;19:11; (c) Woo EM, Ko TY. Colloid Polym Sci 1996;274:309; (d) Zhou C, Clough SB. Polym Eng Sci 1988;28:65.
- [22] (a) Kim HG, Robertson RE. J Polym Sci Part B Polym Phys 1998;36:1417; (b) Qudah AMA, Raheil AA. Polym Int 1995;38:375; (c) Nichols ME, Robertson RE. J Polym Sci Part B Polym Phys 1992;30:755; (d) Stein RS, Misra RS. J Polym Sci Part B Polym Phys 1980;18:327; (e) Cheng SZD, Pan R, Wunderlich B. Makromol Chem 1988;189:2443; (f) Yeh JT, Runt J. J Polym Sci Part B Polym Phys 1989;27:1543.
- [23] Passingham C, Hendra PJ, Cudby MEA, Zichy Z, Weller M. Eur Polym J 1990;26:631.
- [24] Srinivas S, Caputo FE, Graham M, Gardner S, Davis RM, McGrath JE, et al. Macromolecules 1997;30:1012.
- [25] (a) Marand H, Velikov V. J Therm Anal 1997;49:375; (b) Verma RK, Velikov V, Kander RG, Marand H. Polymer 1996;37:5357; (c) Verma R, Marand H, Hsiao B. Macromolecules 1996;29:7767; (d) Jonas AM, Russell TP, Yoon DY. Macromolecules 1995;28:8491; (e) Hsiao BS, Sauer BB, Verma RK, Zachmann HG, Seifert S, Chu B, et al. Macromolecules 1995;28:6931; (f) Hsiao BS, Gardner KH, Wu DQ, Chu B. Polymer 1993;34:3986; (g) Kroger KN, Zachmann HG. Macromolecules 1993;26:5202; (h) Marand H, Prasad A. Macromolecules 1992;25:1731; (i) Lee Y, Porter RS, Lin JS. Macromolecules 1989;22:1756; (j) Deslandes Y, Day M, Sabir NF, Suprunchuk T. Polym Compos 1989;10:360; (k) Lee Y, Porter RS. Macromolecules 1987;20:1336; (l) Cheng SZD, Cao MY, Wunderlich B. Macromolecules 1986;19:1868.
- [26] Yasuniwa M, Tsubakihara S, Satou T, Iura K. J Polym Sci Part B Polym Phys 2005;43:2039.
- [27] Yasuniwa M, Tsubakihara S, Sugimoto Y, Nakafuku C. J Polym Sci Part B Polym Phys 2004;42:25.
- [28] Yasuniwa M, Satou T. J Polym Sci Part B Polym Phys 2002;40:2411.
- [29] Yoo ES, Im SS. J Polym Sci Part B Polym Phys 1999;37:1357.
- [30] Denchev Z, Nogales A, Sics I, Ezquerro TA, Belta-calleja FJ. J Polym Sci Part B Polym Phys 2001;39:881.
- [31] Wang Y, Bhattacharya M, Mano JF. J Polym Sci Part B Polym Phys 2005;43:3077.
- [32] Kong Y, Hay JN. Polymer 2003;44:623.
- [33] Hobbs SY, Pratt CF. Polymer 1975;16:462.
- [34] Medellin-Rodriguez FJ, Phillips PJ, Lin JS, Campos R. J Polym Sci Part B Polym Phys 1997;35:1757.
- [35] Papageorgiou GZ, Bikiaris DN. Polymer 2005;46:12081.
- [36] Pyda M, Wunderlich B. J Polym Sci Part B Polym Phys 2000;38:622.
- [37] Sinha Ray S, Okamoto K, Okamoto M. Macromolecules 2003;36:2355.
- [38] Bourbigot S, Gilman JW, Wilkie CA. Polym Degrad Stab 2004;84:483.
- [39] Lim ST, Hyun YH, Choi HJ, Jhon MS. Chem Mater 2002;14:1839.
- [40] Zhu J, Morgan AB, Lamelas FJ, Wilkie CA. Chem Mater 2001;13:3774.
- [41] Zong R, Hu Y, Wang S, Song L. Polym Degrad Stab 2004;83:423.
- [42] Kissinger HE. Anal Chem 1957;29:1702.